LANGMUIR TURBULENCE UNDER HURRICANE GUSTAV

by

Tyler J. Rabe

A thesis submitted to the Faculty of the University of Delaware in partial fulfillment of the requirements for the degree of Master of Science in Ocean Engineering

Fall 2013

LANGMUIR TURBULENCE UNDER HURRICANE GUSTAV

by

Tyler J. Rabe

Approved: _____
Tobias Kukulka, Ph.D.
Professor in charge of thesis on behalf of the Advisory Committee

Approved: _____
Mark A. Moline, Ph.D.
Director of the School of Marine Science and Policy

Approved: _____
Nancy M. Targett, Ph.D.
Dean of the College of Earth, Ocean, and Environment

Approved: _____
James G. Richards, Ph.D.
Vice Provost for Graduate and Professional Education

ACKNOWLEDGMENTS

Over the past few years I have received excellent support and encouragement from the entire CEOE community. I would like to especially thank my advisor Tobias Kukulka Ph.D. for providing insights and guidance in investigating this complex turbulence problem. Tobias's leadership and knowledge has helped me every step of the way. I also want to thank my committee members Albert D. Kirwan Ph.D. and Fabrice Veron Ph.D. for their support throughout this process, whether it be in the classroom or in a passing conversation. I also wanted to acknowledge Pablo Huq Ph.D. for providing excellent advice and insight related to my research. Lastly, I wanted to acknowledge research funding from the Physical Ocean Science and Engineering (POSE) fellowship.

Without the help from our collaborators Eric D'Asaro and Ramsey Harcourt at The University of Washington, and Isaac Ginis, Tetsu Hara, and Brandon Reichl at The University of Rhode Island, this research would not have been possible. They provided observational data and wave modeling expertise that has been a foundation for this study. I sincerely appreciate all of our discussions that have helped to develop this research.

Thanks to all of my fellow graduate students who have provided valuable scientific and political discussions. I will miss all of our lively debates. I also want to thank the US National Science Foundation (Grant OCE - 1130678) for supporting this research. This research was also supported in part through the use of computational or staff resources provided by Information Technologies at the University of

Delaware. Finally, I want to thank my friends and family for being supportive and motivating throughout graduate school.

TABLE OF CONTENTS

LIST OF FIGURES

ABSTRACT

Extreme winds and complex wave field, which vary in space and time, drive upper ocean turbulence in tropical cyclone conditions. Motivated by Lagrangian float observations of mixed layer averaged (i.e. bulk) vertical kinetic energy (VKE) under Hurricane Gustav, upper ocean turbulence is investigated based on large eddy simulation (LES) of the wave-averaged Navier-Stokes equations. The wave-driven residual current (Stokes drift) interacts with the sheared Eulerian currents to create Langmuir circulations, whose wide range of temporal and spatial scales characterizes them as a type of turbulence. To realistically capture wind and wave-driven Langmuir turbulence (LT), the LES model imposes the Stokes drift vector from spectral wave simulations; both, the LES and the wave model are forced by the NOAA HRD surface wind analysis product (H*WIND). Results strongly suggest that without LT effects, simulated VKE underestimates the observed VKE. LT increases the VKE indicating that it plays a significant role in upper ocean turbulence dynamics. Consistent with observations, the LES predicts a suppression of VKE near the hurricane eye due to wind-wave misalignment. However, this decrease is weaker and of shorter duration than that observed, potentially due to large scale horizontal advection not captured in our LES. LES results agree better with observations for smaller wind stresses, suggesting that the air-sea drag coefficient is lower that previously estimated in high wind tropical cyclone conditions. Both observations and simulations are consistent with a highly variable upper ocean turbulence field beneath tropical cyclone cores. Bulk VKE, a TKE budget analysis, and anisotropy coefficient (ratio of horizontal to

vertical velocity variances) profiles all indicate that LT can suppress turbulence to levels closer to that of shear turbulence (ST) due to misaligned wind and wave fields. VKE approximately scales with the directional surface layer Langmuir number that incorporates the wind stress and Stokes drift vectors and the upper ocean boundary layer depth. Such a scaling provides guidance for the development of an upper ocean boundary layer parametrization that explicitly depends on sea state. Enhanced mixing from LT leads to greater sea surface temperature (SST) changes under the hurricane core, which can provide a direct negative feedback on tropical cyclone strength.

Chapter 1

INTRODUCTION

Over the past few decades, forecasts for tropical cyclone track have improved significantly with the development of complex numerical models. However, the ability to predict their strength has not progressed as quickly [Bender and Ginis, 2000, Emanuel et al., 2004]. This is partially due to the incomplete understanding of turbulent upper ocean mixing. Extreme winds and complex wave fields drive upper ocean turbulence, which entrains cooler water from the thermocline to induce significant cooling of the sea surface [Price, 1981]. Cooling, in turn, reduces the heat fluxes that drive tropical cyclones [Emanuel et al., 2004].

Many studies (e.g. [Price et al., 1986, Large et al., 1994, Zedler et al., 2002]) have investigated the impact of high winds on upper ocean turbulence using one dimensional turbulence parametrizations. They focus on the importance of inertially rotating wind stress on mixing at the thermocline. Resonance between the wind and the Eulerian currents can amplify the currents and increase the shear at the base of the mixed layer. Typically, there is a rightward bias in entrainment effects due to this resonance [Price, 1981, Skyllingstad et al., 2000]. The one dimensional parametrizations used in these models do not explicitly include the effects of surface gravity waves, which have been shown to play an important role in upper ocean mixing [McWilliams et al., 1997, Li et al., 2005].

Non-breaking ocean surface waves influence turbulence through their interaction with the sheared Eulerian currents. Specifically, the phase averaged effects

of surface gravity waves lead to a net drift (Stokes drift) which tilts vertical vorticity into the direction of wave propagation, creating wind aligned roll vortices, called Lagngmuir circulations [Langmuir et al., 1938]. Craik and Leibovich [1976] developed the mathematical theory describing Langmuir circulations, based on wave current interactions. The spectrum of temporal and spatial scales exhibited by Langmuir circulations has characterized them as a type of turbulence, or Langmuir turbulence (LT) [McWilliams et al., 1997]. Many studies (e.g. [Plueddemann et al., 1996, McWilliams et al., 1997, Li et al., 2005, Kukulka et al., 2009]) have shown that LT is a dominant feature of upper ocean turbulence. A common model used to study LT is large eddy simulations (LES), which are based on the Craik-Leibovich equations [Skyllingstad and Denbo, 1995, McWilliams et al., 1997].

Traditional LES studies have consisted of simulating turbulence in wind wave equilibrium conditions utilizing a Stokes drift profile from a monochromatic wave field (e.g. [McWilliams et al., 1997, Li et al., 2005, Polton and Belcher, 2007]). However, in tropical cyclone conditions, wind and wave fields are rapidly changing and both fields can be significantly misaligned. Some LES studies have investigated the effects of inertially rotating winds with prescribed wave fields [Skyllingstad et al., 2000], LT under various wind and wave age equilibrium conditions [Harcourt and D'Asaro, 2008], comparison of LES with non-stationary field observations [Kukulka et al., 2009, 2010, 2013], and wind wave misalignment conditions [Van Roekel et al., 2012]. More recently, Sullivan et al. [2012] investigated the importance of LT under an idealized tropical cyclone using a combined approach between a wave and LES model. They found that LT was a dominant feature of the upper ocean with significant spatial and temporal variability. The complex Stokes drift profiles from the spectral wave simulations resulted in significant misalignment between the wind and the Stokes drift at various depths, leading to weaker LT on the left side of the storm.

The strength of the LT was shown to be highly dependent on the local evolution of the wind and wave state.

Over the past two decades, in situ observations under tropical cyclones have become more frequent with the development of profiling and Lagrangian floats. Air deployed profiling floats were first developed to investigate the ocean response to tropical cyclone events [Sanford et al., 1987, Shay et al., 1992]. More recently, Lagrangian floats have been used to measure vertical velocities, gas concentrations, and mixed layer evolution [D'Asaro et al., 1996, D'Asaro, 2003a,b, D'Asaro and McNeil, 2007]. Lagrangian floats roughly track particle trajectories and thus can be used to measure turbulence properties during a passing tropical cyclone. Recent observations from Hurricane Gustav by Eric D'Asaro have motivated this current study.

In this study, field measurements of mixed layer averaged (i.e. bulk) vertical kinetic energy (VKE) from Lagrangian floats are compared with simulated bulk VKE from an LES model. The modeling procedure will be similar to that of Sullivan et al. [2012] but with wind and wave fields from Hurricane Gustav (not idealized). The goals of this study are to better understand the importance of LT under tropical cyclones, determine whether or not wind wave misalignment is a critical factor for the strength of turbulence, and to determine whether turbulence parametrizations need to explicitly depend on waves.

Chapter 2

OBSERVATIONS UNDER HURRICANE GUSTAV

Three Lagrangian floats were deployed by Eric D'Asaro from the Applied Physics Laboratory at the University of Washington during Hurricane Gustav. The floats, which roughly track water parcels, measured vertical velocities over a 12 hour period spanning from day 245.1 to 245.6 of year 2008. Each float was deployed in a different region of Gustav to examine the spatial variability in the turbulence. The floats will be referred to as the Edge, Eye, and Peak floats, corresponding to their locations relative to Gustav (refer to Figure 2.1). The deployment location of the floats was approximately 100 - 150 km off of the coast of Louisiana. The floats operate within the mixed layer and generally sample down to the mixed layer base. From these measurements, the bulk VKE was determined [D'Asaro et al., 1996, D'Asaro, 2003a]. A correction factor has been applied to the bulk VKE measurements to account for the unresolved turbulence due to the finite float size [D'Asaro et al., 1996]. Bulk vertical kinetic energy is a proxy for LT and will help identify whether or not LT effects are important during tropical cyclones.

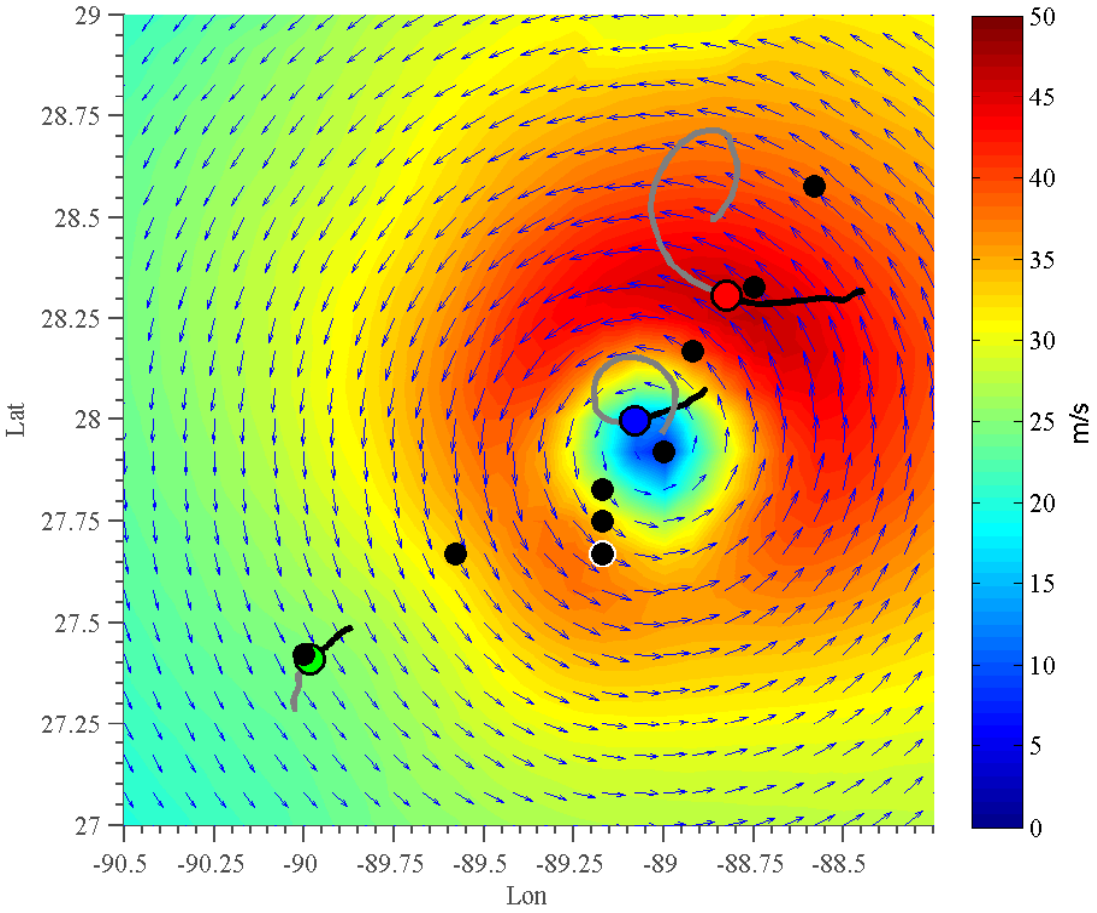

Figure 2.1: Wind field for Hurricane Gustav at yearday 245.27 produced from NOAA H*Wind. Colors represent the magnitude of the 10 m wind speed ($|U_{10}|$) in ms^{-1}. Wind vectors are overlaid on the wind magnitude color plot. Wind vectors are scaled relative to the maximum wind. At this time, Gustav is translating at approximately 9 ms^{-1} to the NW. The location of the three Lagrangian floats are indicated with colored dots with a black outline. The Edge, Eye, and Peak float are represented in green, blue, and red respectively. The black/gray lines represent the track of the floats before/after day 245.27. Black dots represent stationary locations. The black dot with a white outline is location 409 which is investigated in detail in Section 4.3.

Figure 2.2 displays the observed bulk VKE from the three floats (thick lines) and the corresponding value for u_*^2 (dashed lines). For the Edge float and the Peak float, the bulk VKE roughly tracks with u_*^2. However, the Eye float does not track with u_*^2 after the eye of Hurricane passes over the float. Although u_*^2 for the Peak and the Eye float are roughly the same at day 245.35, the bulk VKE is drastically different. This suggests that there is a significant suppression of turbulence behind the hurricane eye. These bulk VKE measurements are compared with results from large eddy simulations to examine this suppression and to better understand the importance of LT under tropical cyclones.

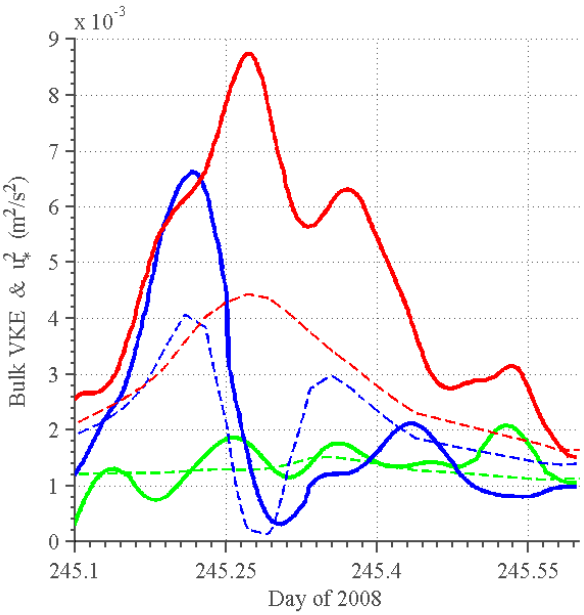

Figure 2.2: Observed bulk VKE for the Edge (green), Eye (blue), and Peak (red) floats (compare to float locations in previous figures). The thick lines are the observations and the dashed lines are the wind stress divided by the density $\tau/\rho = u_*^2$.

Chapter 3

LARGE EDDY SIMULATIONS UNDER HURRICANE GUSTAV

To model the ocean turbulence observed by the three Lagrangian floats, an LES model was used in concert with a wave model similar to the approach by Sullivan et al. [2012]. Unlike any previous approaches, the LES and wave models are forced with a NOAA wind product to realistically capture the wind and wave field of Hurricane Gustav.

3.1 LES Model

Large eddy simulations rely on the assumption that small scale turbulence generally obeys some universal characteristics that can be parametrized. LES models are able to resolve the large scale, energy containing, turbulent motion while avoiding the extremely high computational cost of resolving the small dissipation scale eddies. The LES model filters out the subgrid eddies and parametrizes these eddies based on the universal characteristics of turbulence in the inertial sub-range. The governing LES equations, based on the equations by Craik and Leibovich [1976], for the resolved scale motion are [McWilliams et al., 1997],

$$\frac{\partial \overline{u}_i}{\partial t} + \epsilon_{ijk}\overline{\omega}_j\overline{u}_k + \epsilon_{ijk}f_j(\overline{u}_k + u_{s,k}) = -\frac{\partial \overline{\pi}}{\partial x_i} + \frac{\overline{\rho}}{\rho_o}g_i + \epsilon_{ijk}u_{s,j}\overline{\omega}_k + \frac{\partial \tau_{ij}}{\partial x_j} \qquad (3.1)$$

$$\frac{\partial \overline{\rho}}{\partial t} + (\overline{u}_j + u_{s,j})\frac{\partial \overline{\rho}}{\partial x_j} = \frac{\partial \tau_{\rho j}}{\partial x_j} \tag{3.2}$$

$$\frac{\partial \overline{u}_i}{\partial x_i} = 0, \tag{3.3}$$

where the rotational form of the nonlinear advective term in the momentum equation is used. All terms with an overbar denote resolved variables (i.e. filtered over the grid scale).

The index $i = (1, 2, 3)$ represents the three coordinate directions (x, y, z), where x is East, y is North, and z is upward. The velocity vector (u, v, w) corresponds to the indexed velocity components (u_1, u_2, u_3). The Coriolis vector $(f_1, f_2, f_3) = (0, 0, f)$ where f is the Coriolis parameter corresponding to a particular latitude. The gravitational acceleration vector is given by $(g_1, g_2, g_3) = (0, 0, -g)$ where $g = 9.81$ ms^{-2}. The vorticity $\overline{\omega}_i$ is equal to $\epsilon_{ijk}\frac{\partial \overline{u}_k}{\partial x_j}$ where ϵ_{ijk} is the Levi-Civita permutation tensor. The Stokes drift vector is $(u_{s,1}, u_{s,2}, u_{s,3}) = (u_s, v_s, 0)$. The pressure term $\overline{\pi} = \frac{p}{\rho_o} + \frac{1}{2}[(u_i + u_{s,i})(u_i + u_{s,i})]$ is a generalized pressure that includes the kinetic energy, which appears when the nonlinear advective term is written in rotational form. To capture buoyancy effects, the Boussinesq approximation was used with a constant reference density of ρ_o. Density and temperature are linearly related through the thermal expansion coefficient

$$\alpha = -\frac{1}{\rho}\left(\frac{\partial \rho}{\partial T}\right). \tag{3.4}$$

A constant thermal expansion coefficient of $\alpha = 2 \times 10^{-4}$ K^{-1} is used. In reality, seawater density is a function of temperature and salinity. As a simplification, the

temperature and salinity effects have been combined based on the expansion coefficients and typical temperature and salinity ranges.

The subgrid scale stresses for momentum and density are τ_{ij} and $\tau_{\rho j}$ respectively. The subgrid scale stress for density is linearly related to temperature through the thermal expansion coefficient. The subgrid scale fluxes are parametrized via eddy viscosities for both momentum and temperature (i.e. ν_M and ν_T). The subgrid scale model is explained in detail in Appendix A.

Langmuir circulation dynamics are captured through the Stokes drift vorticity interaction term, $\mathbf{u}_s \times \omega$. The irrotational shear generated by the surface waves acts to tilt vertical vorticity perturbations into the Stokes drift propagation direction. This leads to a series of coherent counter-rotating vortices that align roughly with the wind [McWilliams et al., 1997].

3.2 Surface Fluxes

The primary forcing for both the LES model and the wave model is the 10 m atmospheric winds. NOAA's Hurricane Research Division (HRD) has developed a product available for hurricane forecasters that enables them to obtain realistic wind fields in near real time. This product is widely used by the science and engineering communities [Powell et al., 1998]. It is referred to as H*Wind or HRD Wind. The H*Wind project re-creates a wind field from a particular tropical cyclone using all available observational data. This includes satellite data, dropsondes, buoy measurements, and measurements from hurricane eyewall penetrating flights. The result is a composite wind velocity at 10 m height. The wind fields are available at three hour intervals throughout a tropical cyclones translation. To use the H*Wind predictions, the wind fields are linearly interpolated between "known" wind fields to provide constant realistic forcing for the wave and LES models. A full description of the

H*Wind product is described by Powell et al. [1998] and an example of a wind field reconstruction, using H*Wind, from Hurricane Katrina can be seen in Powell et al. [2010].

The driving mechanism for the LES model is the surface momentum flux. The surface momentum flux is parametrized via the bulk formula

$$\tau = \rho_a C_d \mathbf{U}_{10} |\mathbf{U}_{10}|, \tag{3.5}$$

where ρ_a is the air density and $\mathbf{U}_{10}$ is the two component wind vector referenced to 10 m height. For moderate winds below 20 ms^{-1} the drag coefficient C_d is parametrized using the formulation from Large and Pond [1981], where

$$C_d = \begin{cases} 0.0012 & |\mathbf{U}_{10}| < 11\text{ms}^{-1} \\ (0.49 + 0.065|\mathbf{U}_{10}|) \times 10^{-3} & 11\text{ms}^{-1} < |\mathbf{U}_{10}| < 25\text{ms}^{-1} \end{cases} \tag{3.6}$$

In high wind and misaligned wind and wave conditions, the air-sea momentum flux mechanisms are incompletely understood and the drag coefficient is not well constrained [Powell et al., 2003, Donelan et al., 2004, French et al., 2007, Sanford et al., 2011, Holthuijsen et al., 2012]. Following Sullivan et al. [2012], the drag coefficient is saturated at $C_d = 1.8 \times 10^{-3}$ above wind speeds of 20 ms^{-1}. Field and laboratory studies by Powell et al. [2003], Donelan et al. [2004], and French et al. [2007] have shown that for very high wind speeds, the drag coefficient reaches a saturated value. Donelan et al. [2004] showed that this saturated drag coefficient was approximately 2.3×10^{-3} and an ocean momentum budget analysis from Sanford et al. [2011] showed a lower value of 1.4×10^{-3}. More recently, Holthuijsen et al. [2012] investigated the effects of wind wave misalignment on the drag coefficient. They showed that the orientation of the wind and the swell waves can influence the drag

coefficient significantly.

For all simulations a dynamically insignificant constant surface cooling of -5 Wm^{-2} is imposed to facilitate the turbulence spin-up from rest [McWilliams et al., 1997]. The air-sea heat flux during Hurricane Gustav is likely larger than -5 Wm^{-2}; however, surface heat fluxes contribute little to the overall cooling of the mixed layer and to mixed layer turbulence generation under tropical cyclones. The primary mechanism by which the mixed layer is cooled is entrainment of cooler water from the base of the mixed layer, accounting for greater than 90% of the total cooling [Price, 1981, Sullivan et al., 2012].

3.3 Wave Forcing

To generate time dependent wave spectra a third generation wave model is deployed, WAVEWATCH III (WW3) [Tolman, 2009], which has been modified previously to better match with observed hurricane wave fields by Isaac Ginis, Tetsu Hara, and Brandon Reichl at the University of Rhode Island, who provide wave model output. WW3 solves the spectral wave action equation for the directional frequency spectra (i.e. $F(\omega, \theta)$). The model accounts for wave dissipation due to whitecapping, wave-bottom interactions, non-linear wave-wave interactions, and wind input, which is driven by H*Wind.

The wave model domain spans from 18° to 31°N in latitude and -98° to 80°W in longitude to encompass the area with the Lagrangian float observations (Figure 2.1). The latitude and longitude are spaced by $1/12°$ in each direction to adequately capture the highly variables changes around the eye of the storm.

The wave spectrum in the model is discretized into 24 direction and 40 intrinsic or relative frequencies. The direction is linearly spaced from 0 to 2π. The frequencies span from 0.0285 Hz to 1.1726 Hz with a logarithmic spacing of $f_{n+1} = 1.1 f_n$ where n

is the nth frequency. The intrinsic frequency is related to the wavenumber through the dispersion relation for deep water waves. Above a frequency of 1.1726 Hz an empirical spectral tail, which decays with a slope of k^{-4}, is applied to account for short waves that are not resolved by the model. The spectral tail accounts for an additional 22 frequencies, resulting in 62 total frequencies.

The wind forcing from H*Wind is interpolated using "normalized interpolations" ([Fan et al., 2009]) between the 3 hour spaced H*Wind wind fields to obtain the 30 minute wind fields. The wave simulation uses a time step of 300 seconds. This transient wind field then drives the wave model and produces the time and space dependent wave spectrum $F(\omega, \theta)$. The wave spectra are then used to calculate the Stokes drift profiles via

$$\mathbf{u_s}(z) = 2 \int_0^{\infty} \int_{-\pi}^{\pi} \mathbf{k}\omega F(\omega, \theta) e^{2|\mathbf{k}|z} d\theta d\omega. \tag{3.7}$$

To match the dynamic time step of the LES model to the fixed time step for the Stokes drift profiles and wind forcing, a simple linear interpolation is used.

3.4 LES Setup

For all simulations a domain of $(L_x, L_y, L_z) = (300, 300, 120)$ m is used with a total of $(N_x, N_y, N_z) = (256, 256, 228)$ grid points. This corresponds to a horizontal resolution Δx and Δy of 1.17 m and a vertical resolution Δz is 0.52 m with a grid anisotropy ratio of 2.23. Sensitivity tests of grid resolution and domain size have shown that the chosen configuration adequately captures the turbulence (Appendix B).

The initial upper ocean density structure for the simulations are determined

from in situ measurements. The three Lagrangian floats were designed with a vertical profiling mode to allow them to measure the ocean state before and after the storm passes. Before the floats were in Lagrangian drift mode (day 245.1 to 245.6), they were able to take vertical profiles of salinity, temperature, and various gas concentrations. Figure 3.1 shows the initial potential density profiles (solid) from the three floats as well as the initial profiles used for the Lagrangian float simulations (dashed) that are used as initial conditions. A linear gradient of density is used to represent the density structure. The mixed layer and density gradient are estimated based on the observations.

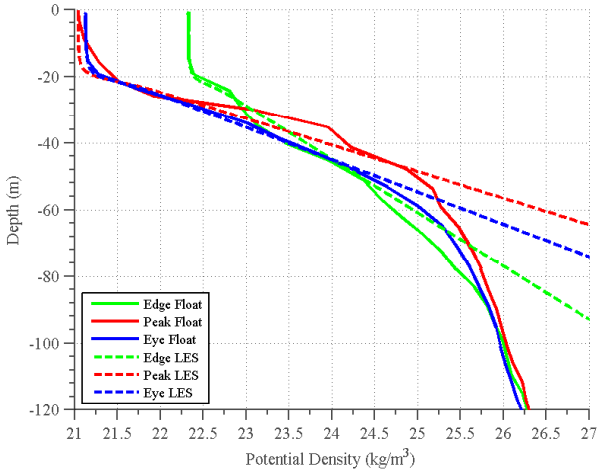

Figure 3.1: Potential density profiles for the three floats (solid) and the initial density profiles used in the LES model (dashed). Profiles were taken at day 245.083.

To initialize the transient simulations, first stationary simulations are generated for each individual case. Each simulation is run with the wind, wave, and initial density profiles for multiple eddy turnover times (h/u_*) or until stationary turbulent

statistics are reached. At this point, the turbulent fields from the stationary simulations are used to initialize the transient simulations. This includes the fields of velocity, temperature, generalized pressure, and SGS turbulent kinetic energy. The time varying wind and Stokes drift profiles are applied to the LES simulations to force the turbulence. The simulations are run for approximately 12 physical hours for the Lagrangian floats simulations and 37 physical hours for the stationary locations. To examine the importance of the wave field on the turbulence in the upper ocean, simulations are run with and without the Stokes drift. These cases will be referred to as Langmuir turbulence (LT) and shear turbulence (ST) respectively.

3.5 Simulated Locations

Study locations were chosen perpendicular to the translation direction of Gustav to best understand the spatial variability of the turbulence across the track of Gustav. Gustav passed from the southeast to the northwest (Figure 2.1). Nine stationary locations and three Lagrangian float "locations" are chosen (Figure 2.1). To simulate the turbulence at each stationary location, local wind and wave forcing is imposed.

To determine space and time dependent forcing conditions for the Lagrangian floats, bilinear interpolations were utilized. The interpolated 10 m wind speed, the significant wave height, and the wind direction for the Edge (green), Eye (blue), and Peak (red) floats are displayed in Figure 3.2. The misalignment angle θ_{ww} between the wind direction and the Stokes drift direction at various depths

$$\cos(\theta_{ww}(t,z)) = \frac{\mathbf{U}_{10}(t)\cdot\mathbf{u}_s(t,z)}{|\mathbf{U}_{10}(t)||\mathbf{u}_s(t,z)|}, \tag{3.8}$$

highlights the directional variability in the Stokes drift profile with depth (Figure

3.3).

The Edge float (green), to the left of Gustav's eye, experiences relatively constant wind forcing throughout the Lagrangian measurement period (day 245.1 to 245.6). Throughout this time, the wind direction at the Edge float changed by 90°. The significant wave height, related to the strength of the Stokes drift, changes from 7.5 m to below 5 m when the wind direction is shifting. Figure 3.3 panel (a) shows that the shift in wind direction causes the Stokes drift profiles to become misaligned with the wind. The Eye float (blue) experiences the most variable forcing conditions. The wind speed reaches a peak around 45 ms^{-1} and has a rapid reduction around day 245.25 followed shortly by an increase in the wind speed. This is due to the hurricane translating over the float and the float moving directly into the hurricane eye (Figure 2.1). As the wind speed is rapidly changing, the wind direction is also shifting by 180°. These rapidly changing conditions have strong effects on the significant wave height, which changes from 12.5 m at day 245.2 to 5 m around day 245.3. These changes cause the Stokes drift profiles to become almost 180° misaligned with the winds (Figure 3.3 panel (b)). The Peak float experiences very consistent strong forcing throughout the 12 hour observation period as indicated in Figure 3.2 (red). The wind speed reaches approximately 50 ms^{-1} and the significant wave height 15 m. The wind direction changes slowly by approximately 90°. As seen at the Edge and Eye float, the significant wave height has a rapid drop off as the storm passes over the Peak float. However, the Stokes drift profiles remain relatively aligned with the wind direction (Figure 3.3 panel (c)). Note that for some locations the wind speed remains relatively constant, but the wind and wave misalignment significantly changes (e.g. station 409, compare forcing in Figure 3.2 (black curves) with Figure 3.3 (d)).

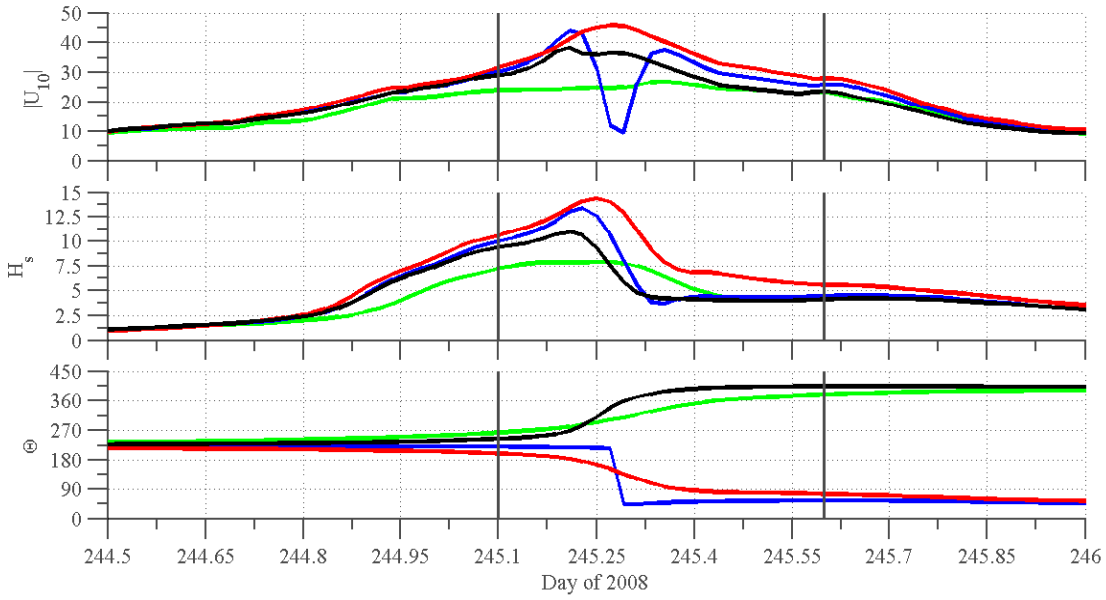

Figure 3.2: Forcing conditions for the three Lagrangian floats and location 409. The top, center, and bottom panels show the magnitude of the 10 m wind speed, the significant wave height, and the wind direction respectively. The wind direction is oriented in the traditional x-y space with 0° being E. The Edge, Eye, and Peak floats are represented in green, blue, and red. Location 409 is represented in black. The vertical gray lines indicate the float measurement period from day 245.1 to 245.6.

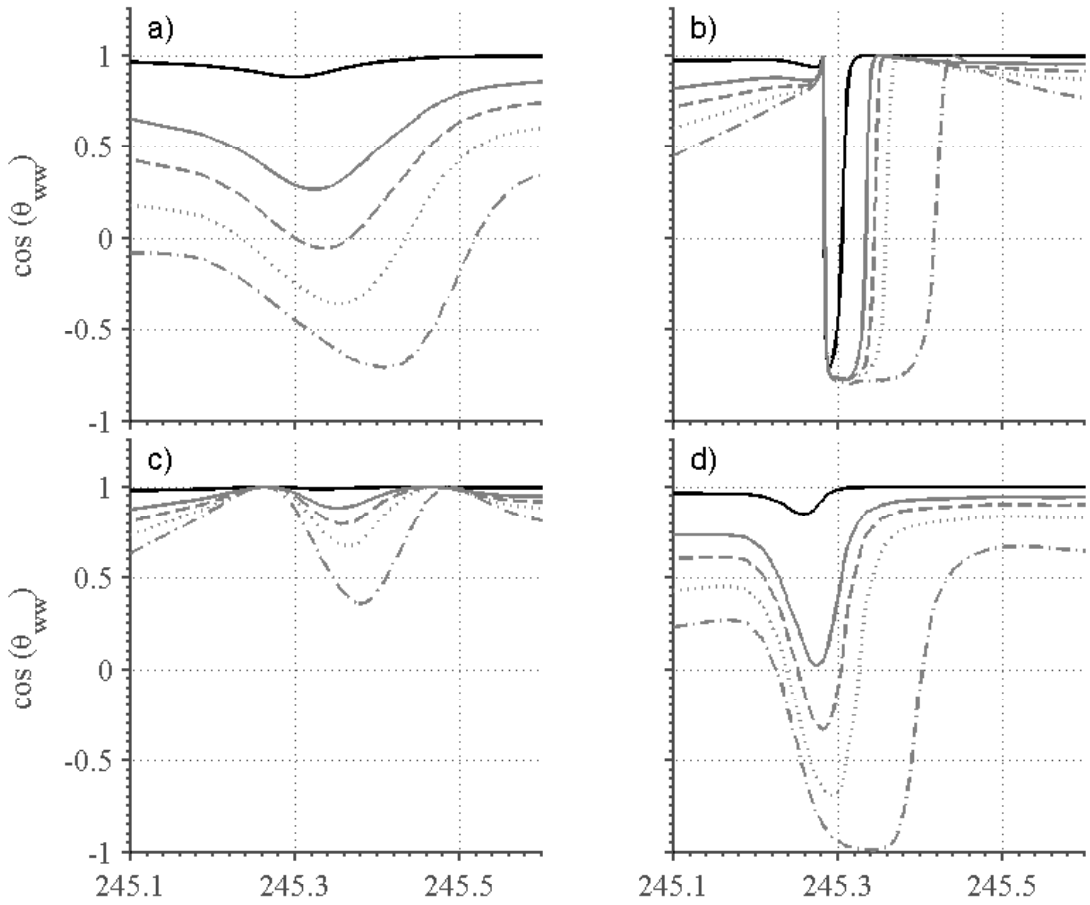

Figure 3.3: Misalignment angle between the wind and the Stokes drift given by Equation 3.8 for the Edge float (a), the Eye float (b), the Peak float (c), and location 409 (d). The misalignment angle is shown at the surface (black) and at depths z = (4.74, 10, 19.47, 59.47) m (gray: solid, dash, dotted, dash-dot). The misalignment is shown over the period of day 245.1 to 245.6.

Chapter 4

RESULTS

4.1 Comparison With Observations

In order to assess the model performance, mixed layer averaged VKE, which plays a key role in vertical mixing and transport, is compared with observations. In particular, the importance of LT during tropical cyclones is assessed, and the effects of wind and wave misalignment on the suppression of turbulence is investigated.

The total, i.e. resolved plus unresolved SGS contributions, LES bulk VKE is calculated via

$$\left\langle w_T'^2 \right\rangle_h = \frac{1}{h} \int_{-h}^{0} \left(\left\langle w'^2 \right\rangle + \left\langle w_{SGS}'^2 \right\rangle \right) dz, \tag{4.1}$$

where h is the mixed layer depth and "T" represents total VKE including the subgrid scale VKE. The angle brackets denote horizontally averaged quantities from the three dimensional LES output.

For the Edge float the observed bulk VKE (green) falls between the simulation results for LT (solid black) and ST (solid gray) (Figure 4.1 (a)). There is considerable variability in the observations, spanning between the simulation results for LT and ST. Relatively constant bulk VKE levels are expected at this location because the wind speed is almost constant and only turns gradually (green curves Figure 3.2). The variability in the LT simulation results is generally influenced by the strength of the Stokes drift profile (inferred from significant wave height in Figure 3.2 (green)).

The misalignment between the wind and the Stokes drift only changes gradually and thus does not drive the variability for the LT simulations (Figure 3.3 (a)).

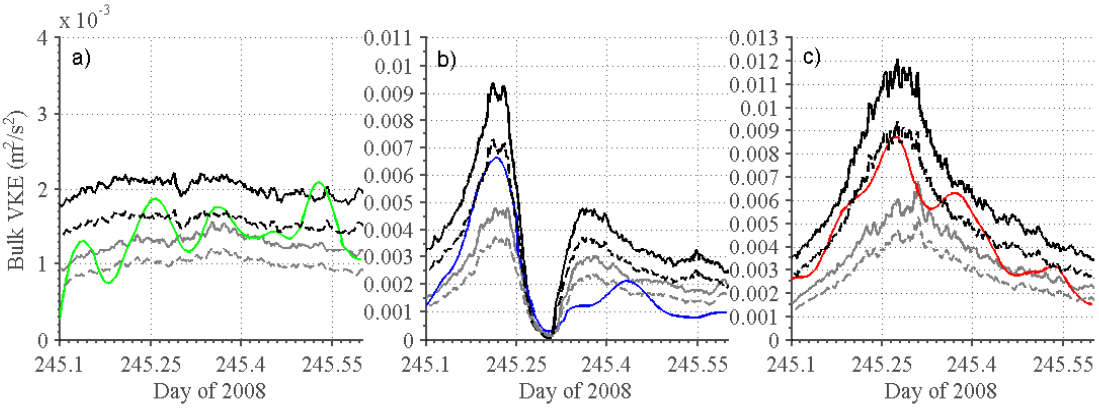

Figure 4.1: Bulk VKE comparison between simulations and observations for the Edge (a), Eye (b), and Peak (c) floats. The green, blue, and red lines are the observations, the solid black lines are the LES results for LT, and the solid gray lines are the LES results for ST. The dashed black/gray lines are estimated VKE based on a lower saturated drag coefficient of $C_d = 0.0014$.

The Eye float experiences the most variable forcing conditions (blue lines Figure 3.2) and, accordingly, VKE levels are also highly variable (Figure 4.1 (b)). Before the eye of the storm passes over the float the observed bulk VKE level falls in between the levels predicted with the ST and LT simulations. However, as the storm's eye passes over the float around day 245.3, the observed bulk VKE suddenly falls below the levels predicted by both the ST and LT simulations and remains low for the rest of the measurement period. The simulations capture a suppression of turbulence, but it is not as strong or as long as observed. Possible reasons for this discrepancy are discussed below.

The Peak float experiences very consistent strong wind and wave forcing throughout the 12 hour observation period (red lines Figure 3.2). Similar to the Edge float results, the observed bulk VKE (red) falls in between the LT (solid black) and ST (solid gray) (Figure 4.1 (c)).

The observations and LES comparisons of bulk VKE reveal three important insights on upper ocean turbulence under tropical cyclones. First, overall (except for the Eye float after day 245.3), the observed bulk VKE for all three floats falls in between the Langmuir and shear LES results. This suggests that LT is important during tropical cyclones. Although there is considerable variability in the measurements, the observed elevated VKE cannot be obtained without the addition of the Craik-Leibovich vortex force. Second, the simulations for LT systematically overpredict the observations, which may be due to an incorrect parametrization of the drag coefficients in high winds and complex seas. Third, although the simulations capture significant suppression of turbulence due to surface waves (discussed below), it is unlikely that LT alone caused the strong suppression of turbulence measured by the Eye float after day 245.3.

4.2 Modeling Uncertainties

Measurements and the modeling approach contain uncertainties that contribute to the differences between simulation results and the observations. The Lagrangian floats were deployed during extreme wind and wave conditions which provide formidable experimental challenges. Measurement uncertainties are systematically assessed by Eric D'Asaro (personal communication). Here, modeling uncertainties are focused on.

4.2.1 Basic Wave and LES Approach

Modeling uncertainties are associated with wave field predictions and the LES model assumptions. The wave model, based on the wave action equation, makes approximations for wave action source terms. Wave input and wave dissipation are not well understood in complex wind conditions typical of tropical cyclones. Nevertheless, the wave model has been tested previously in hurricane conditions (e.g. [Fan et al., 2009]) and results agree with observations. Therefore, wave field uncertainty is unlikely to play a significant role in the errors. The LES model employs a subgrid scale model with turbulence closure assumptions. However, the solution to the LES equations is likely insensitive to the subgrid parametrization because the turbulence is well resolved (greater than 85%)[Pope, 2000]. Domain size and grid resolution also play an important role in the solutions accuracy. However, sensitivity tests revealed that a large domain size and higher spatial resolution do not significantly change the results presented here (Appendix B).

4.2.2 Breaking Waves

Breaking waves, which inject turbulent kinetic energy (TKE) at the ocean surface [Melville, 1996, Terray et al., 1996], are not explicitly captured in the modeling approach. Previous observational studies (e.g. Terray et al. [1996]) for wind-wave equilibrium conditions indicate that the breaking wave effect is mainly confined to the surface and does not significantly influence the bulk mixed layer dynamics that is the focus of this study. LES studies by Noh et al. [2004] and Sullivan et al. [2007] suggest that breaking waves may interrupt Langmuir circulation structure close to the surface, but do not strongly influence bulk VKE. Finally, it is theoretically not well understood how to include stochastic wave breaking events in the Craik Leibovich equations, which have been originally derived for turbulent motion that is

significantly weaker and slower than the motion of breaking waves. Clearly, the breaking wave effect is an important unknown that needs to be addressed in future studies.

4.2.3 Three Dimensional Effects

The LES approach does not capture any lateral effects, such as Ekman pumping or large scale horizontal advection. To assess such three dimensional effects, preliminary results of a three dimensional regional ocean model based on the Reynolds-averaged hydrostatic equations of motion under Hurricane Gustav is investigated. Results indicate that the ocean restratifies below the eye due to vertical advection of the thermal field likely due to Ekaman pumping, which is consistent with the upper ocean response observed and modeled under Hurricane Frances [Sanford et al., 2011]. If this stratification suppresses upper ocean turbulence it may contribute to the low VKE levels observed by the Eye float after the passing of the storm.

When the ocean restratifies under the eye, the mixed layer shoals to roughly 10 m (based on 3D RANS results) and becomes comparable in depth to the significant wave height of approximately 5 m (blue line Figure 3.2 center). If breaking wave effects penetrate roughly to a depth consistent with the significant wave height, this could significantly disrupt LT structure and reduce the bulk VKE. It is important to note that only part of the wave spectrum, which is actively forced by the wind, contributes to breaking waves and thus the penetration depth is likely less than the significant wave height. Furthermore, when the eye passes over the float, the wind speed rapidly increases to above $30 ms^{-1}$ which likely leads to significant breaking wave events which inject bubbles into the mixed layer. Bubbles have been shown to enhance the near surface stratification and suppress turbulence [Smith, 1998,

Gemmrich, 2012]. These combined effects could lead to reduced bulk VKE levels consistent with observations.

4.2.4 Drag Coefficient

Finally, the drag coefficient uncertainty in high wind ([Powell et al., 2003, Donelan et al., 2004]) and complex wave conditions ([Holthuijsen et al., 2012]) is another important factor influencing the differences between the observed and simulated bulk VKE. Recent analysis of ocean momentum budgets have indicated that the drag coefficient C_d under tropical cyclones with wind speeds from 30-47 ms^{-1} is approximately 1.4×10^{-3} [Sanford et al., 2011]. Holthuijsen et al. [2012] describe a large range in drag coefficient, based on an analysis of boundary layer wind profiles. They found that the orientation of the wind and the swell waves can reduce the drag coefficient to 1×10^{-4}, i.e. smaller than the value used in this study. Assuming that the bulk VKE is proportional to the wind stress, a drag coefficient from the simulations can be estimated. Using $C_d = 0.0014$ from Sanford et al. [2011], estimated bulk VKE reduces (dashed black/gray lines in Figure 4.1). The LT simulations (dashed black) agree well with observations suggesting that the drag coefficient at wind speeds above 30 ms^{-1} may be less than the chosen saturated value of 0.0018. Although the simulation results agree much better with the observations with a lower drag coefficient, the suppression observed by the Eye float is still stronger than a lower drag coefficient can explain. It is likely that the combined effects of the modeling uncertainties could lead to low bulk VKE levels consistent with the observations behind the eye of Gustav.

Given the aforementioned complexities of the tropical cyclone system and the straightforward approach without any adjustments to enhance the agreement between observations and simulations, the comparison is overall surprisingly good

and encouraging. In particular the results suggest that LT plays a significant role under tropical cyclones and critically influences upper ocean turbulence variability.

4.3 Variability of Upper Ocean Turbulence Under Tropical Cyclones Due to LT

To further investigate the spatiotemporal variability of the upper ocean turbulence in response to complex wind and wave conditions, the LES results for the nine fixed locations across the track of Gustav are investigated (Figure 2.1). Before presenting the results for all locations, a single location (Location 409, Figure 2.1) that highlights the strong variability in LT is first investigated.

4.3.1 In Depth Analysis of a Single Location

Location 409 is located to the left of the eye of Gustav near the radius of maximum winds. This location experiences very consistent wind forcing with highly variable changes in the wave field. The wind speed time series at location 409 is almost symmetric with respect to the time of maximum winds, at which the wind speed is approximately 40 ms^{-1} (Figure 3.2). The significant wave height increases as the storm approaches and then quickly subsides, similar to the forcing conditions experienced by the Peak float. The misalignment during this period is relatively strong and persistent (Figure 3.3 (d)). Particularly important are the surface misalignment and the misalignment at $z = -4.74$ m which contribute significantly to the Stokes drift shear production term in the TKE budget. As noted earlier, misalignment in the wave field can have drastic impacts on the VKE in the mixed layer [Van Roekel et al., 2012].

To assess the importance of the wave field on the VKE, the VKE (including SGS) normalized by u_*^2 will be investigated. The normalization removes the dependence on the changes in wind stress magnitude and allows for an investigation into the impacts of the wave field and the changing wind direction.

From day 245.1 to 245.6, which is the dynamically interesting time range when the wave field is rapidly changing, LT has significantly enhanced VKE relative to ST, as expected (Figure 4.2, LT simulation (a) and ST simulation (b)). The ST simulation shows relatively consistent normalized VKE levels suggesting a VKE scaling with u_*^2. There is a slight reduction in the normalized ST VKE level around day 245.25. This can be attributed to the changing wind direction, which results in adjusting upper ocean turbulence (compare with Figure 3.2). The LT simulation however shows a drastic reduction in the normalized VKE around day 245.25. This can be attributed to combined effects of the changing wave field and the misalignment between wind and wave directions.

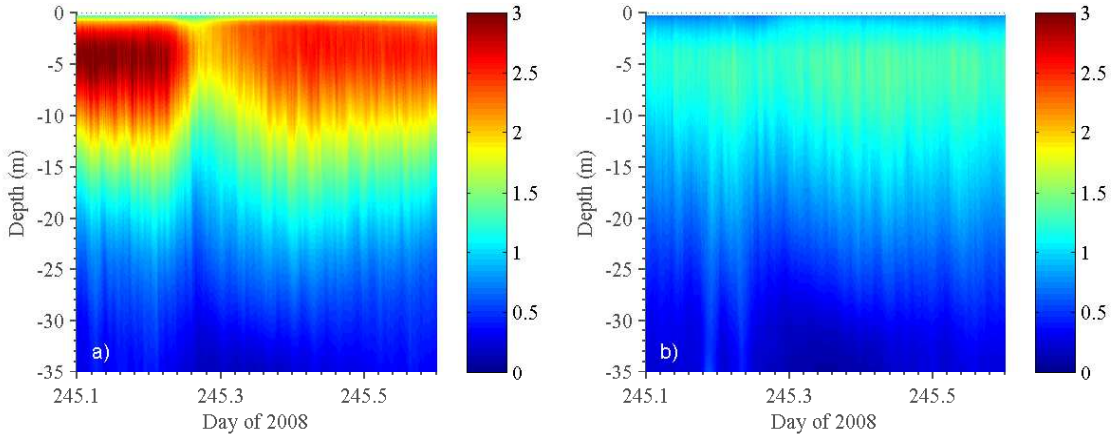

Figure 4.2: Normalized vertical kinetic energy (w'^2/u_*^2) for LT (a) and ST (b) cases between day 245.1 to 245.6.

To assess the magnitude of the changes in normalized VKE, and determine the importance of the wave field on the variability of the turbulence, the bulk VKE for the Langmuir turbulence simulation is scaled relative to the bulk VKE for the shear simulation (Figure 4.3). In spite of significant wind and wave misalignment, waves always enhance VKE. Before day 245.25 the LT bulk VKE is twice that of the ST bulk VKE. As Gustav's eye passes location 409 the wind-wave misalignment changes rapidly (Figure 3.3 (d)), so that around day 245.25, the scaled bulk VKE decreases from 2.25 to 1.5 very rapidly. This suggests that turbulence can be suppressed by the effects of the surface gravity waves from strong LT to a near ST regime. This drastic wave dependent change suggests that upper ocean turbulence parametrizations employed in TC ocean models need to be dependent on the directional wave field. In order to capture this significant variability, LT must be considered.

Figure 4.3: Bulk VKE from the LT simulation $\left\langle w'^2_{LC} \right\rangle_h$ scaled relative to the bulk VKE from the ST simulation $\left\langle w'^2_S \right\rangle_h$.

To more fully understand these rapid changes in the bulk VKE seen above, the horizontally averaged TKE budgets for the ST and LT simulations are investigated. This will provide insight into the effects of the changing wave conditions on the turbulence. The horizontally averaged resolved TKE equation is

$$\frac{\partial(k)}{\partial t} = -\left\langle u_i' w' \right\rangle \frac{\partial \langle u_i \rangle}{\partial z} - \left\langle u_i' w' \right\rangle \frac{\partial u_{s,i}}{\partial z} + \frac{\left\langle w' \rho' \right\rangle}{\rho_o} g - \frac{\partial}{\partial z}\left(\left\langle \frac{1}{2} u_i' u_i' w' \right\rangle + \frac{\left\langle w' p' \right\rangle}{\rho_o} \right) - \langle \epsilon \rangle + SGS \quad (4.2)$$

where $k = 1/2 \left\langle u_i' u_i' \right\rangle$ is the resolved turbulent kinetic energy (for a more complete discussion of TKE budgets, see, e.g. Skyllingstad et al. [2000]). Each resolved variable can be broken down into a horizontal mean and a deviation from the mean via

$\overline{u}_i = \langle u_i \rangle + u_i^{'}$. The angle brackets denote horizontally averaged quantities. The terms in Equation 4.2 from left to right are the temporal rate of change of resolved turbulent kinetic energy per unit mass (per unit mass will be neglected herein for brevity), resolved TKE Eulerian shear production, Stokes drift shear production, resolved buoyancy flux, vertical gradient of resolved vertical TKE flux, vertical gradient of pressure work, and dissipation. Sugrid scale terms are denoted as SGS. Since the simulation results are well resolved (approximately 85%), SGS terms are not explicitly included in the budgets.

The instantaneous TKE budget will be examined at two specific time points for LT and ST simulations to highlight the differences in the energetics before and during the misalignment of the wave field. The first time point is at day 245.115 when the wind and wave field are relatively well aligned and the wind speed is still increasing (black line Figure 3.2 top). The wind speed is approximately 30 ms^{-1} at this time and the wind direction has not started to shift (Figure 3.2). The second time point is at day 245.285 when the wave field is highly misaligned and the wind direction is shifting (Figure 3.2). At this time the wind speed is approximately 35 ms^{-1}.

At day 245.115 the TKE budget for the ST simulation displays a balance between Eulerian mean shear production and dissipation between the surface and $z/h = -0.25$ (Figure 4.4 (b)). The divergence of vertical TKE flux also plays a small role near the surface. Below $z/h = -0.25$ the budget is a balance between mean shear production, dissipation, and buoyancy flux. This is consistent with shear driven boundary layers. In contrast, the LT results in panel (a) display three important distinctions from the ST result; the Stokes drift shear production is a dominant term through the upper half of the mixed layer, the Eulerian shear production is small except near surface and near the mixed layer base, and the budgets are considerably

more complex. It is also important to note that the vertical gradient of vertical TKE flux (thin gray line) is significantly enhanced in the LT simulation relative to the ST simulation. This is caused by Langmuir circulations increasing the vertical transport of highly energetic turbulence to the base of the mixed layer. The peak in the Eulerian shear production near the base of the mixed layer is characteristic to LT, which efficiently transports and homogenizes horizontal momentum throughout the mixed layer to enhance shear locally at the mixed layer base [Kukulka et al., 2010]. At day 245.115 LT clearly plays a key role in TKE budgets.

In contrast to the TKE budget at day 245.115, at day 245.285, when wind and waves are misaligned the LT and ST results are more similar to one another (Figure 4.4 (c/d)). Below $z/h = -0.25$ both the LT and ST TKE budgets display a dominant balance between mean shear production and dissipation. In the region between $z/h = 0$ to -0.25 the Stokes drift shear production (panel (c)) again plays an important role in the TKE budget for the LT simulation. The misalignment in the wave field caused the Stokes drift shear production to decrease significantly. The Stokes drift shear production only penetrates to a depth of $z/h = -0.25$ which is much shallower than the TKE budget displays at day 245.115. The similarity between panel (c) and (d) suggest that the LT simulation has transitioned toward a shear driven turbulence regime because of the misaligned wave field. Thus, the transient wave response to a rapidly turning wind field determines the upper ocean turbulence characteristics under tropical cyclones.

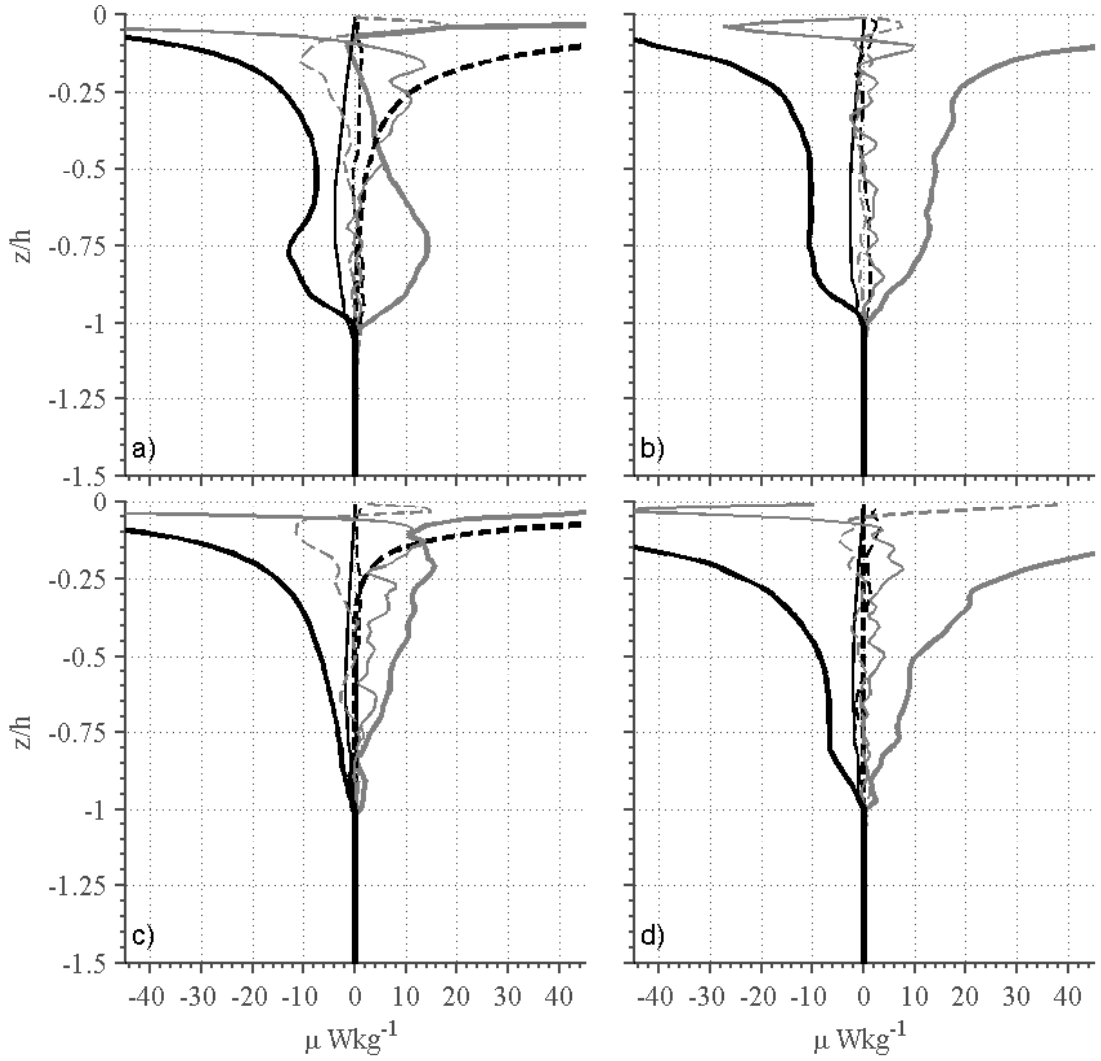

Figure 4.4: TKE budget for the LT (a/c) and ST (b/d) cases at day 245.115 (a/b) and 245.285 (c/d). The thin black dashed line represents the time rate of change of total TKE, the thick solid gray line represents the resolved mean shear production, the thick black dashed line (in panels (a/c) only) represents the Stokes drift shear production, the thin solid black line represents the resolved buoyancy production, the thin solid gray line represents the vertical flux of resolved TKE, the thin gray dashed line represents the vertical pressure work, and the thick solid black line represents the dissipation. Refer to Equation 4.2.

It is useful to investigate the alongwind, crosswind, and vertical velocity variance profiles to diagnose LT from ST. If the wind blows in the x direction, typical ordering of the variances away from the surface for ST are $\langle u_T'^2 \rangle > \langle v_T'^2 \rangle > \langle w_T'^2 \rangle$ and for LT are $\langle w_T'^2 \rangle > \langle u_T'^2 \rangle > \langle v_T'^2 \rangle$ [McWilliams et al., 1997, Polton and Belcher, 2007]. Since in the hurricane simulations the wind direction is constantly changing, profiles of the turbulent anisotropy coefficient [Polton and Belcher, 2007] are examined, which is defined as

$$R_t = \frac{\langle w_T'^2 \rangle}{\langle u_T'^2 \rangle + \langle v_T'^2 \rangle}. \tag{4.3}$$

If R_t is 0.5 then the turbulence is isotropic turbulence, if it is less that 0.5 it is shear driven, and if R_t is greater than 0.5 the turbulence is Langmuir driven. Figure 4.5 shows the turbulent anisotropy coefficient for the LT (black curves) and ST (gray curves) simulation results at day 245.115 (solid) and day 245.285 (dashed) corresponding to the TKE budgets in Figure 4.4. At day 245.115 the profile indicates very strong LT (solid black) with R_t approaching 0.8 at a $z/h = -0.2$. In contrast, the profiles for the ST (solid gray) show values less than 0.2. At day 245.285 the R_t profiles for LT (dashed black) indicate that the turbulence has become more isotropic or shear generated with a peak in R_t of 0.5. The profile for the LT case at day 245.285 (dashed black) still indicates some Langmuir activity (i.e. subsurface peak around $z/h = -0.1$) however it is significantly weaker than before. The ST anisotropy profile (dashed gray) for the later time point indicate strong ST with a maximum in R_t of 0.3. This result is consistent with the TKE budget results shown above and confirms that the effects of the misaligned wave field can change the characteristics of the turbulence from a LT regime to a ST regime.

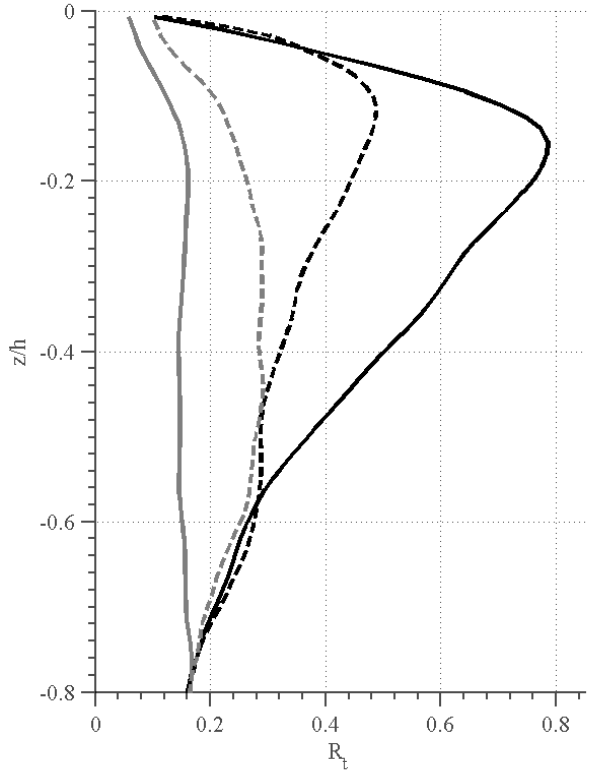

Figure 4.5: Turbulent anisotropy coefficient R_t ([Polton and Belcher, 2007]) at day 245.115 (solid lines) and day 245.285 (dashed lines) for the LT (black) and ST (gray) cases.

Horizontal cross section of vertical velocity normalized by u_* at the depth of maximum R_t (above $z/h = -0.5$) for the LT and ST simulations support the TKE budget and R_t profile results that indicate a transition from LT to ST (Figure 4.6). Normalized vertical velocities are much more organized and stronger with LT (left panels) than without (right panels). At day 245.285 the LT (panel (c)) and ST (panel (d)) contours indicate that the vertical velocities are more similar with significantly weakened LT (panel (c)). Although the LT is weakened relative to results from day 25.115 (panel (a)), the flow structures in panel (c) are more organized than those from

day 245.285 without LT (panel (d)), indicating that the LT has not fully transitioned to ST, but rather significantly weakened.

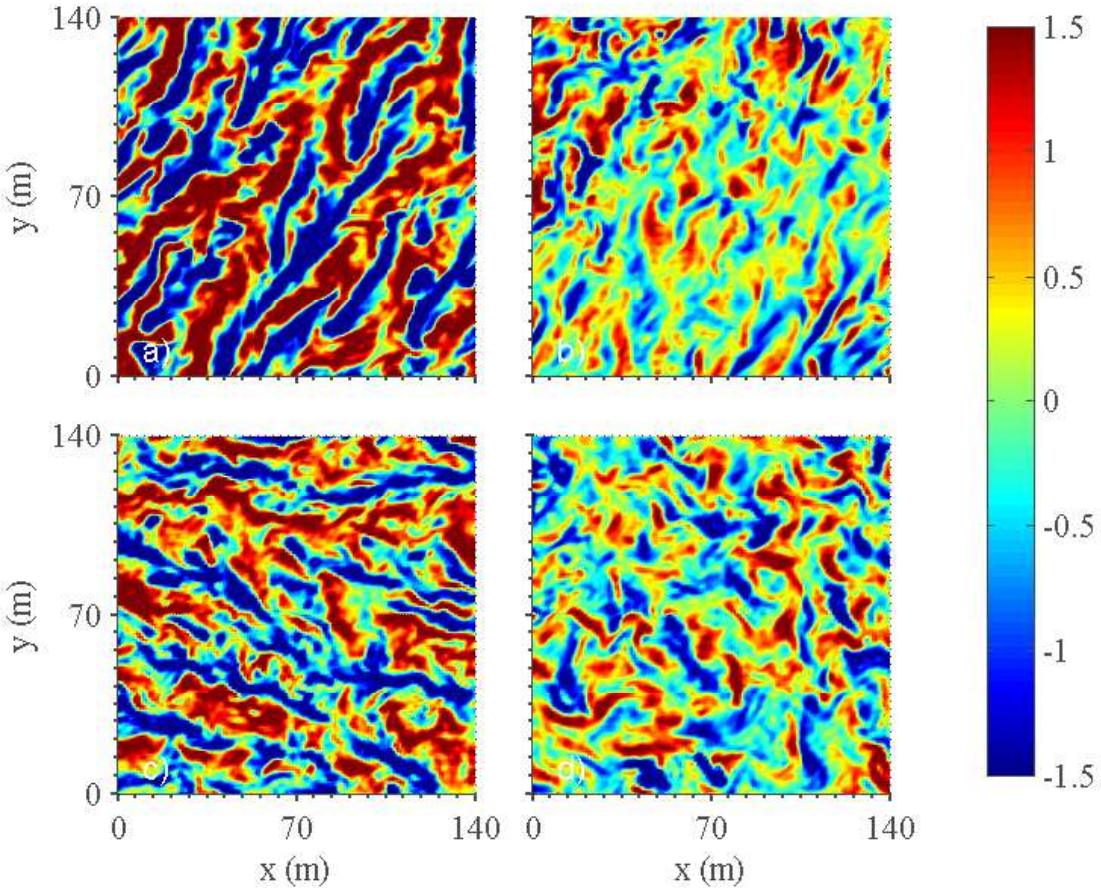

Figure 4.6: Cross sections of vertical velocity normalized by u_* at day 245.115 (a/b) and 245.285 (c/d) for the LT (a/c) and ST (b/d) simulations. Cross sections are taken at the depth of maximum anisotropy coefficient R_t above $z/h = -0.5$.

The investigation of turbulence characteristics at a single station reveals that, first, LT always enhances VKE levels in the mixed layer relative to ST. Second, the wave field can influence drastic changes in bulk VKE (Figures 4.2 and 4.3), especially

in close proximity to the eye. Finally, LT simulation results indicate that the characteristics of turbulence can approach those of ST through wind wave misalignment. Next, the spatial and temporal variability of turbulence across the track of Gustav is investigated by examining all simulated locations.

4.3.2 Langmuir Number Scaling

To obtain a broader view of the turbulence response of the upper ocean, the results from all nine stationary locations as well as the three float simulations will be investigated. In particular, the interest is in how the turbulent Langmuir number ($La_t = \sqrt{u_*/|\mathbf{u}_s(0)|}$) affects the normalized bulk VKE. The turbulent Langmuir number has traditionally been used to describe LT and to develop scalings for vertical mixing.

The definition of the surface layer Langmuir number from Van Roekel et al. [2012] and Harcourt and D'Asaro [2008] is utilized here. It incorporates the misalignment between the wind and the Stokes drift as well as the Lagrangian shear direction. This modified Langmuir number projects the surface stress and the Stokes drift into the Lagrangian shear direction, which has been shown to predict the Langmuir circulation direction by Van Roekel et al. [2012], via

$$La_{SL*} = \sqrt{\frac{u_* \cos\left(|\alpha_L - \Theta|\right)}{|\langle \mathbf{u}_s \rangle_{0.2h}| \cos\left(|\alpha_L - \Theta_S|\right)}} \tag{4.4}$$

where α_L is the Lagrangian shear direction, Θ_S is the Stokes drift direction, and Θ is the wind direction. The Stokes drift and Stokes drift direction have been averaged over 20 % of the mixed layer as outlined by Harcourt and D'Asaro [2008]. The

Lagrangian shear direction is calculated via

$$\tan\left(\alpha_L\right) = \frac{\langle \partial v_L/\partial z \rangle_{0.2h}}{\langle \partial u_L/\partial z \rangle_{0.2h}}, \tag{4.5}$$

where u_L and v_L are the Lagrangian velocities in the x and y direction. Since the Lagrangian shear is a function of z, α_L is averaged over 0.2 of the mixed layer to allow for one angle in the Langmuir number formulation. The surface layer Langmuir number in Equation 4.4 is plotted relative to the normalized bulk VKE. Directionality is also included in the normalized bulk VKE via

$$\frac{\left\langle w_T'^2 \right\rangle_h}{\left(u_* \cos\left(\alpha_L - \Theta\right)\right)^2},$$

which projects the friction velocity u_* into the Lagrangian shear direction. The simple surface layer Langmuir number from Harcourt and D'Asaro [2008] is also examined

$$La_{SL} = \sqrt{\frac{u_*}{|\langle \mathbf{u}_s \rangle_{0.2h}|}} \tag{4.6}$$

and scaled relative to the normalized bulk VKE $\left\langle w_T'^2 \right\rangle_h / u_*^2$ to investigate how important the misalignment is for the Langmuir number scaling.

Scaling the normalized bulk VKE with the modified Langmuir number, indicate that if directionality is included in the formulation, the results scale better (Figure 4.7 (a/b)). During the time of maximum misalignment (day 245.2 to 245.4) the simple surface layer Langmuir number has many outliers (panel (a)). Most of those are removed when misalignment is taken into account (panel (b)). For the beginning and end of the simulations, when the wind and waves are relatively aligned, directionality is not as important. This suggests that the surface layer Langmuir number with directionality is an important parameter to parametrize LT during

TC's. Some deviations from the scalings are expected because the simulations are fully transient where the previous scalings from Harcourt and D'Asaro [2008] and Van Roekel et al. [2012] have been developed with steady state simulation results. Note that the data before and after the eye of Gustav passes have slight biases (Figure 4.7 (b)). Before the eye passes, the data (solid dots) fall almost on top of the scalings from Van Roekel et al. [2012]. After the eye passes, the results (crosses) fall above the scalings. One explanation for the differing scaling results before/after Gustav passes over the locations are history effects associated with transient forcing, and differences in strongly forced and decaying turbulence. After the wind begins to reduce, the residual turbulence remains in the mixed layer longer than the changing forcing. Next, entrainment effects under Gustav will be investigated, thus highlighting the need for a wave dependent scaling for TC ocean models.

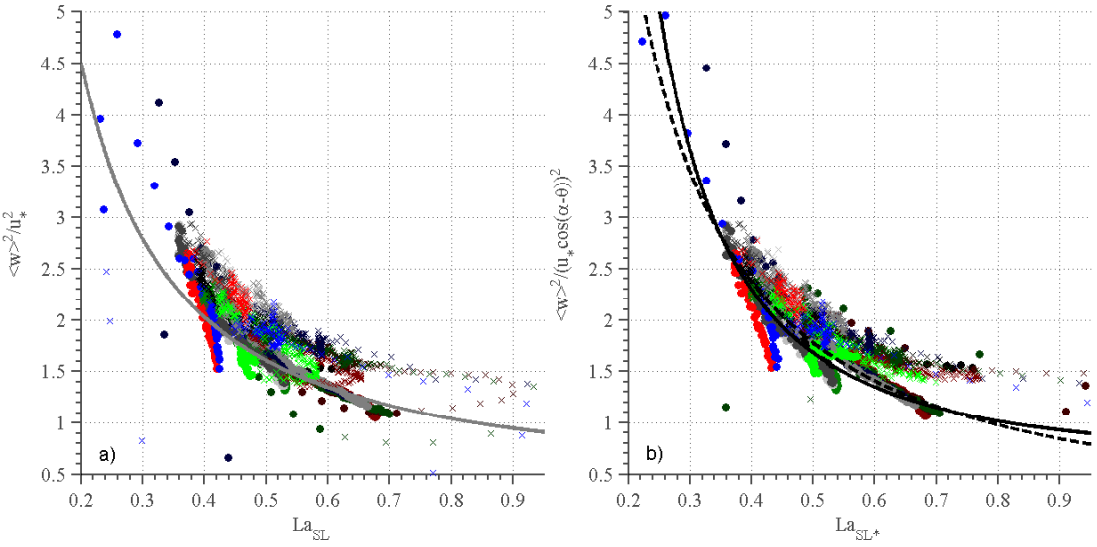

Figure 4.7: Surface layer Langmuir number from Van Roekel et al. [2012] (b) and the simple surface layer Langmuir number from Harcourt and D'Asaro [2008] (a) scaled relative to the bulk VKE normalized by u_* or the projected u_*. All LT stationary simulation results and float simulation results are included. Time points before the eye of Gustav passes the location are solid circles and time points after are indicated with crosses. Also included are three proposed scalings from Van Roekel et al. [2012] (black: solid and dashed) and Harcourt and D'Asaro [2008] (gray) for the surface layer Langmuir number.

4.3.3 Implications for Mixed Layer Base Entrainment

Finally, the sea surface temperature changes for the LT and ST simulations are examined to better understand the importance of LT on mixed layer temperature changes. Two stationary locations were investigated in this analysis. One location is to the right of the eye and the other to the left of the eye, similar to Sullivan et al. [2012].

Results indicate that the entrainment effects to the right (dashed curves) of the eye are much more significant than the left (solid curves) of the eye (Figure 4.8).

This is due to the resonance between the winds and the Eulerian currents as well as the alignment between the wind and wave field [Price, 1981, Skyllingstad et al., 2000, Sullivan et al., 2012]. The entrainment effects to the left are smaller due to off-resonance and misalignment. These results show that LT produce stronger mixing at the thermocline than ST, with LT being as much a 1° C cooler than ST. More importantly, this strong temperature difference occurs at the time when the eye is passing over the locations at day 245.3, providing a direct negative feedback to the hurricane core. Based on an analysis of tropical cyclones from 1975 - 2002, sea surface temperature changes greater than 1°C can lead to roughly 40% reduction in enthalpy flux [Cione and Uhlhorn, 2003]. Including LT in coupled TC ocean models is important for improving TC strength predictions.

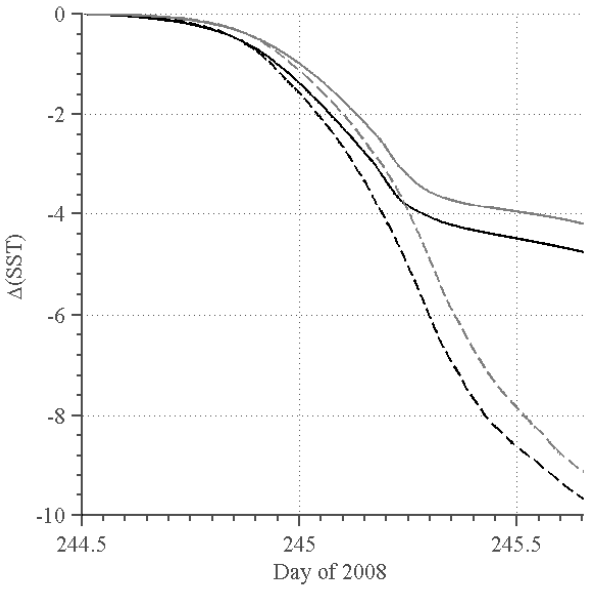

Figure 4.8: Time series of the sea surface temperature changes. The solid curves are the location to the left of the eye and the dashed curves are to the right of the eye. Black indicates simulation results for LT and gray indicates results for ST.

Chapter 5

CONCLUSIONS

A large eddy simulation was used to model the turbulence under Hurricane Gustav in an effort to better understand the importance of LT during tropical cyclones. A rational and straightforward approach has been used to simulate the upper ocean response. NOAA's H*Wind was used to produce the time dependent wind fields. WAVEWATCH III was used in concert with the wind fields to produce a time and space dependent wave field. Previous wind stress and drag coefficient parametrizations were used to drive the wave and LES models.

Comparison of LES results with Lagrangian float field observations indicate that LT plays an important role in upper ocean mixing. Results strongly suggest that without LT effects, simulated VKE underestimates the observed VKE. Langmuir turbulence increases the VKE indicating that it plays a significant role in upper ocean turbulence dynamics. Consistent with observations, the LES predicts a suppression of VKE near the hurricane eye due to wind-wave misalignment. However, the observed suppression is stronger and of longer duration than the simulations indicate. Drag coefficient uncertainty, restratification under the eye, and breaking waves with bubble injection could play a role in reducing bulk VKE levels consistent with the observed suppression. LES results agree better with observations with a lower saturated drag coefficient, suggesting that the air-sea drag coefficient is relatively low in tropical cyclone conditions. Bulk VKE, a TKE budget analysis, and anisotropy

coefficients of turbulent velocities all indicate that LT can suppress turbulence to levels closer to that of ST due to wave field variability.

Scaling the normalized bulk VKE versus the surface layer Langmuir number from Harcourt and D'Asaro [2008] and from Van Roekel et al. [2012] shows that misalignment between wind and waves is important for the strength of LT. The data indicate that the addition of directionality in the surface layer Langmuir number collapses the data closer to the scaling results from Van Roekel et al. [2012].

Investigation of temperature profile evolution reveals that LT enhances mixed layer deepening, resulting in larger sea surface cooling compared with ST. The difference between the simulated sea surface cooling for LT versus ST is as much as a 1° C difference and cooling occurs earlier and more rapidly with LT than ST, which will have implications for accurately predicting tropical cyclone strength [Emanuel et al., 2004].

This work suggests that LT critically influences upper ocean response during tropical cyclones and must be considered for accurate TC predictions. The surface layer Langmuir number will provide guidance for development of an upper ocean boundary layer parametrization that explicitly depends on sea-state.

BIBLIOGRAPHY

Morris A Bender and Isaac Ginis. Real-case simulations of hurricane-ocean interaction using a high-resolution coupled model: Effects on hurricane intensity. *Monthly Weather Review*, 128(4):917–946, 2000.

Joseph J Cione and Eric W Uhlhorn. Sea surface temperature variability in hurricanes: Implications with respect to intensity change. *Monthly Weather Review*, 131(8):1783–1796, 2003.

Alex D.D. Craik and Sidney Leibovich. A rational model for langmuir circulations. *Journal of Fluid Mechanics*, 73(03):401–426, 1976.

Eric D'Asaro and Craig McNeil. Air–sea gas exchange at extreme wind speeds measured by autonomous oceanographic floats. *Journal of Marine Systems*, 66(1): 92–109, 2007.

Eric A D'Asaro. Performance of autonomous lagrangian floats. *Journal of Atmospheric and Oceanic Technology*, 20(6):896–911, 2003a.

Eric A D'Asaro. The ocean boundary layer below hurricane dennis. *Journal of Physical Oceanography*, 33(3):561–579, 2003b.

Eric A D'Asaro, David M Farmer, James T Osse, and Geoffrey T Dairiki. A lagrangian float. *Journal of Atmospheric and Oceanic Technology*, 13:1230, 1996.

James W Deardorff. Stratocumulus-capped mixed layers derived from a three-dimensional model. *Boundary-Layer Meteorology*, 18(4):495–527, 1980.

JW Deardorff. The use of subgrid transport equations in a three-dimensional model of atmospheric turbulence. *Journal of Fluids Engineering*, 95:429, 1973.

MA Donelan, BK Haus, Nicolas Reul, WJ Plant, M Stiassnie, HC Graber, OB Brown, and ES Saltzman. On the limiting aerodynamic roughness of the ocean in very strong winds. *Geophysical Research Letters*, 31(18), 2004.

Kerry Emanuel, Christopher DesAutels, Christopher Holloway, and Robert Korty. Environmental control of tropical cyclone intensity. *Journal of the atmospheric sciences*, 61(7):843–858, 2004.

Yalin Fan, Isaac Ginis, Tetsu Hara, C Wayne Wright, and Edward J Walsh. Numerical simulations and observations of surface wave fields under an extreme tropical cyclone. *Journal of Physical Oceanography*, 39(9):2097–2116, 2009.

Jeffrey R French, William M Drennan, Jun A Zhang, and Peter G Black. Turbulent fluxes in the hurricane boundary layer. part i: Momentum flux. *Journal of the atmospheric sciences*, 64(4):1089–1102, 2007.

Johannes Gemmrich. Bubble-induced turbulence suppression in langmuir circulation. *Geophysical Research Letters*, 39(10), 2012.

Ramsey R Harcourt and Eric A D'Asaro. Large-eddy simulation of langmuir turbulence in pure wind seas. *Journal of Physical Oceanography*, 38(7):1542–1562, 2008.

Leo H Holthuijsen, Mark D Powell, and Julie D Pietrzak. Wind and waves in extreme hurricanes. *Journal of Geophysical Research: Oceans (1978-2012)*, 117(C9), 2012.

Tobias Kukulka, Albert J Plueddemann, John H Trowbridge, and Peter P Sullivan. Significance of langmuir circulation in upper ocean mixing: Comparison of observations and simulations. *Geophysical Research Letters*, 36(10), 2009.

Tobias Kukulka, Albert J Plueddemann, John H Trowbridge, and Peter P Sullivan. Rapid mixed layer deepening by the combination of langmuir and shear instabilities: A case study. *Journal of Physical Oceanography*, 40(11):2381–2400, 2010.

Tobias Kukulka, Albert J Plueddemann, and Peter P Sullivan. Inhibited upper ocean restratification in nonequilibrium swell conditions. *Geophysical Research Letters*, 2013.

Irving Langmuir et al. Surface motion of water induced by wind. *Science*, 87(2250): 119–123, 1938.

WG Large and S Pond. Open ocean momentum flux measurements in moderate to strong winds. *Journal of physical oceanography*, 11(3):324–336, 1981.

William G Large, James C McWilliams, and Scott C Doney. Oceanic vertical mixing: A review and a model with a nonlocal boundary layer parameterization. *Reviews of Geophysics*, 32(4):363–403, 1994.

Ming Li, Chris Garrett, and Eric Skyllingstad. A regime diagram for classifying turbulent large eddies in the upper ocean. *Deep Sea Research Part I: Oceanographic Research Papers*, 52(2):259–278, 2005.

James C McWilliams, Peter P Sullivan, and Chin-Hoh Moeng. Langmuir turbulence in the ocean. *Journal of Fluid Mechanics*, 334(1):1–30, 1997.

WK Melville. The role of surface-wave breaking in air-sea interaction. *Annual review of fluid mechanics*, 28(1):279–321, 1996.

Chin-Hoh Moeng. A large-eddy-simulation model for the study of planetary boundary-layer turbulence. *Journal of the Atmospheric Sciences*, 41(13):2052–2062, 1984.

AS Monin and AMf Obukhov. Basic laws of turbulent mixing in the surface layer of the atmosphere. *Contrib. Geophys. Inst. Acad. Sci. USSR*, 151:163–187, 1954.

Yign Noh, Hong Sik Min, and Siegfried Raasch. Large eddy simulation of the ocean mixed layer: The effects of wave breaking and langmuir circulation. *Journal of physical oceanography*, 34(4):720–735, 2004.

Albert J Plueddemann, Jerome A Smith, David M Farmer, Robert A Weller, William R Crawford, Robert Pinkel, Svein Vagle, and Anand Gnanadesikan. Structure and variability of langmuir circulation during the surface waves processes program. *Journal of geophysical research*, 101(C2):3525–3543, 1996.

Jeff A Polton and Stephen E Belcher. Langmuir turbulence and deeply penetrating jets in an unstratified mixed layer. *Journal of Geophysical Research: Oceans (1978-2012)*, 112(C9), 2007.

Stephen B Pope. *Turbulent flows*. Cambridge university press, 2000.

Mark D Powell, Sam H Houston, Luis R Amat, and Nirva Morisseau-Leroy. The hrd real-time hurricane wind analysis system. *Journal of Wind Engineering and Industrial Aerodynamics*, 77:53–64, 1998.

Mark D Powell, Peter J Vickery, and Timothy A Reinhold. Reduced drag coefficient for high wind speeds in tropical cyclones. *Nature*, 422(6929):279–283, 2003.

Mark D Powell, Shirley Murillo, Peter Dodge, Eric Uhlhorn, John Gamache, Vince Cardone, Andrew Cox, Sonia Otero, Nick Carrasco, Bachir Annane, et al. Reconstruction of hurricane katrina's wind fields for storm surge and wave hindcasting. *Ocean Engineering*, 37(1):26–36, 2010.

James F Price. Upper ocean response to a hurricane. *Journal of Physical Oceanography*, 11(2):153–175, 1981.

James F Price, Robert A Weller, and Robert Pinkel. Diurnal cycling: Observations and models of the upper ocean response to diurnal heating, cooling, and wind mixing. *Journal of Geophysical Research*, 91(C7):8411–8427, 1986.

Thomas B Sanford, Peter G Black, James R Haustein, James W Feeney, George Z Forristall, and James F Price. Ocean response to a hurricane. part i: Observations. *J. Phys. Oceanogr*, 17(11):2065–2083, 1987.

Thomas B Sanford, James F Price, and James B Girton. Upper-ocean response to hurricane frances (2004) observed by profiling em-apex floats*. *Journal of Physical Oceanography*, 41(6):1041–1056, 2011.

Lynn K Shay, Peter G Black, Arthur J Mariano, Jeffery D Hawkins, and Russell L Elsberry. Upper ocean response to hurricane gilbert. *Journal of Geophysical Research: Oceans (1978–2012)*, 97(C12):20227–20248, 1992.

Eric D Skyllingstad and Donald W Denbo. An ocean large-eddy simulation of langmuir circulations and convection in the surface mixed layer. *Journal of Geophysical Research: Oceans (1978-2012)*, 100(C5):8501–8522, 1995.

Eric D Skyllingstad, WD Smyth, and GB Crawford. Resonant wind-driven mixing in the ocean boundary layer. *Journal of physical oceanography*, 30(8):1866–1890, 2000.

Jerome A Smith. Evolution of langmuir circulation during a storm. *Journal of Geophysical Research*, 103(C6):12649–12668, 1998.

Peter P Sullivan, James C McWilliams, and Chin-Hoh Moeng. A subgrid-scale model for large-eddy simulation of planetary boundary-layer flows. *Boundary-Layer Meteorology*, 71(3):247–276, 1994.

Peter P Sullivan, JAMES C McWilliams, and W Kendall Melville. Surface gravity wave effects in the oceanic boundary layer: Large-eddy simulation with vortex force and stochastic breakers. *Journal of Fluid Mechanics*, 593(1):405–452, 2007.

Peter P Sullivan, James C McWilliams, WK Melville, and Leonel Romero. Transient evolution of langmuir turbulence in ocean boundary layers driven by hurricane winds and waves. *Journal of Physical Oceanography*, 2012.

EA Terray, MA Donelan, YC Agrawal, WM Drennan, KK Kahma, AJ Williams, PA Hwang, and SA Kitaigorodskii. Estimates of kinetic energy dissipation under breaking waves. *Journal of Physical Oceanography*, 26(5):792–807, 1996.

H. L. Tolman. User manual and system documentation of wavewatch-iii, version 3.14. *NOAA/NWS/NCEP/MMAB Technical Note*, 276:194, 2009.

LP Van Roekel, B Fox-Kemper, PP Sullivan, PE Hamlington, and SR Haney. The form and orientation of langmuir cells for misaligned winds and waves. *Journal of Geophysical Research: Oceans (1978-2012)*, 117(C5), 2012.

SE Zedler, TD Dickey, SC Doney, JF Price, X Yu, and GL Mellor. Analyses and simulations of the upper ocean's response to hurricane felix at the bermuda testbed mooring site: 13-23 august 1995. *Journal of Geophysical Research: Oceans (1978-2012)*, 107(C12):1–29, 2002.

Appendix A

SUBGRID SCALE MODEL

The subgrid scale fluxes are related to the resolved scale turbulent field through an eddy viscosity for momentum, ν_M and the strain rate tensor S_{ij}.

$$\tau_{ij} = \nu_M \left(\frac{\partial \overline{u}_i}{\partial x_j} + \frac{\partial \overline{u}_j}{\partial x_i} \right) \tag{A.1}$$

The eddy viscosity, ν_M, depends on the subgrid scale turbulent kinetic energy and the mixing length. The eddy viscosity is

$$\nu_M = 0.1 l e^{1/2}, \tag{A.2}$$

where e is the subgrid scale contribution of the turbulent kinetic energy and l is the mixing length. The mixing length, based on scaling arguments, is determined by the grid spacing of the LES model and the stability of the boundary layer. For neutral or unstable boundary layer conditions the mixing length is defined by the grid resolution $l = \Delta s = (\Delta x \Delta y \Delta z)^{1/3}$. Hover, if the boundary layer is stable, the mixing length is defined as $l = 0.76 e^{1/2} \left(\alpha g \frac{\partial T}{\partial z} \right)^{-1/2}$. For stable stratification the size of eddies can be smaller than the grid spacing and thus a more stringent mixing length has been defined [Deardorff, 1980].

The eddy viscosity for scalars (e.g. temperature) is defined as

$$\nu_T = \left(1 + 2\frac{l}{\Delta s}\right)\nu_M. \tag{A.3}$$

This gives $\nu_T/\nu_M = 1$ as a lower limit when the stratification yields very stable boundary layer conditions. An upper limit of $\nu_T/\nu_M = 3$ is reached for a neutral or unstable boundary layer where scalar mixing is enhanced. The subgrid scale density fluxes $\tau_{\rho j}$ are related to the resolved scales through the subgrid scale temperature fluxes which are parametrized via

$$\tau_{Tj} = \nu_T \frac{\partial T}{\partial x_j}. \tag{A.4}$$

The prognostic equation for the subgrid scale turbulent kinetic energy, described by Deardorff [1973], is defined as follows.

$$\frac{\partial e}{\partial t} + \overline{u}_j \frac{\partial e}{\partial x_j} = \tau_{ij}\frac{\partial \overline{u}_i}{\partial x_j} + \alpha g \tau_{Tj} + \frac{\partial}{\partial x_j}\left(2\nu_M \frac{\partial e}{\partial x_j}\right) - \epsilon \tag{A.5}$$

The terms in Equation A.5, from left to right, are the temporal rate of change of SGS TKE, advection of SGS TKE by the resolved velocity, production of SGS TKE by the resolved shear, SGS buoyancy production, SGS TKE diffusion, and dissipation. The assumption that was made to arrive at the flux divergence term was the down-gradient diffusion assumption [Moeng, 1984].

The dissipation, ϵ, is modeled by

$$\epsilon = \frac{Ce^{3/2}}{l} \tag{A.6}$$

where

$$C = 0.19 + 0.51l(\Delta x \Delta y \Delta z)^{-1/3}. \tag{A.7}$$

The subgrid scale model, near the surface, is modified to better match with Monin-Obuhkov similarity theory [Monin and Obukhov, 1954, Sullivan et al., 1994, Moeng, 1984, McWilliams et al., 1997].

Appendix B

DOMAIN AND GRID RESOLUTION

To ensure that the simulations are not domain size or grid resolution dependent, many additional test cases were performed. Two of those test cases will be discussed here. The Peak float simulation was used to assess the sensitivity because it experienced the strongest wind and wave forcing of all of the cases that were tested. The first test case uses the default number of grid points of $(N_X, N_y, N_z) = (256, 256, 228)$ and a domain with a horizontal extent that is twice that of the default domain, or $(L_x, L_y, L_z) = (600, 600, 120)$. The second test case utilized the standard domain size of $(L_x, L_y, L_z) = (300, 300, 120)$ with half the number of grid points used, or $(N_X, N_y, N_z) = (128, 128, 128)$. These two test cases will be compared to the standard domain and grid resolution described in Section 3.5. Wave effects will be included in this test as well because the turbulent eddies are much larger for Langmuir turbulence than for shear turbulence. The larger eddies will be a more rigorous test on the domain size.

The mixed layer averaged, or bulk, vertical kinetic energy is used to compare the sensitivity tests. The bulk vertical kinetic energy is defined in Equation 4.1. As mentioned earlier, grid resolution will change the fraction of resolved turbulent motion so the subgrid scale motion must be included to compare different resolutions. Figure B.1 displays the results of the vertical kinetic energy for the three compared test cases. Figure B.1 confirms that the results from these three cases do not depend

on grid resolution or domain size. The low resolution (red) run has slightly lower VKE measurements than the two high resolution cases. This is likely due to the highly anisotropic and coarse grid that is used. However, all results are very similar which confirms that the chosen domain size and grid resolution described in Section 3.4 is an appropriate configuration for the simulations.

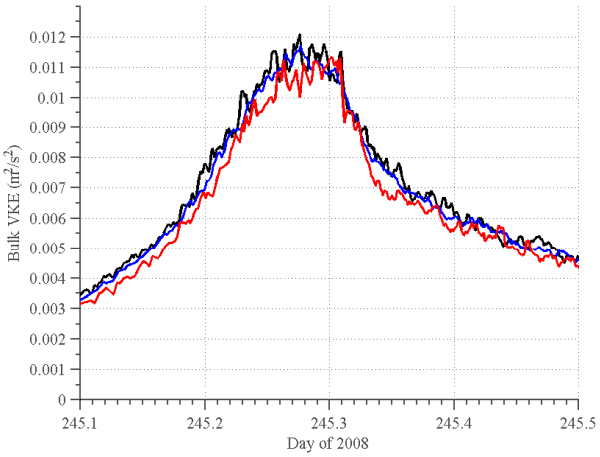

Figure B.1: Comparison of bulk VKE from the standard domain (black), large domain (blue), and low resolution (red).

To investigate whether the LES model resolved the turbulence well, it is useful to look at the relative contribution of the subgrid scale turbulent kinetic energy to the resolved scale turbulent kinetic energy. If the model resolves a large fraction of the turbulent kinetic energy, then the turbulence has not been parametrized via the subgrid model. Typically, if the model resolves 80 percent of the turbulent kinetic energy it is considered a strong solution.

Various factors influence the ability of the LES model to resolve the turbulence. Some of these factors include grid resolution, density stratification, wind speed, and wave forcing. Stratification plays an important role in the determination

of the subgrid scale mixing length, and thus the subgrid scale turbulent kinetic energy (Refer to Appendix A). As the turbulence erodes the thermocline, the stratification becomes stronger and thus the subgrid scale model begins to play a more significant role. The subgrid scale also plays an important role in the vicinity of the surface because the eddies are extremely small in the surface region.

Figure B.2 displays the fraction of resolved TKE for the simulation of location 409 for LT (panel (a)) and ST (panel (b)). Both cases resolve the turbulence very well, away from the surface. Throughout the simulations, 85 to 90 percent is resolved below 5 meters. Near the highly stratified region at the base of the mixed layer, the fraction of resolved TKE is lower and sometimes reaches a value near 0.75. Although this is not considered well resolved, sensitivity tests indicate that the results presented here are independent of the resolution. All simulations, including the float simulations, all resolve between 80 and 90 percent of the turbulent kinetic energy.

The ST simulations are less resolved than the LT simulations because the size of the eddies in shear turbulence are smaller that those in Langmuir turbulence. The energy containing eddies in Langmuir turbulence are very large and are thus very well resolved. This is reflected in the relatively low fraction of parametrized turbulence. The energy containing eddies in the shear turbulence are much smaller and thus are parametrized more frequently by the model. Although the shear turbulence simulations are less resolved than the Langmuir simulations, the results are still very well resolved with the fine grid resolution.

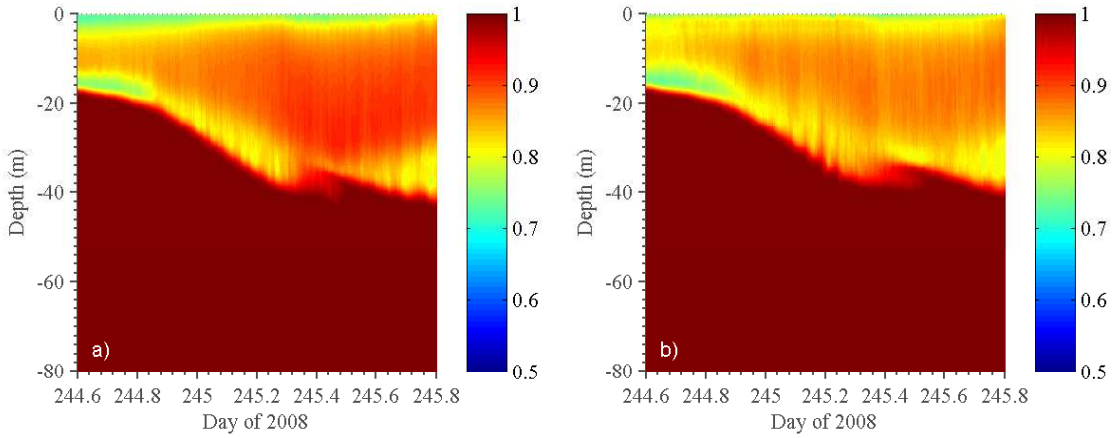

Figure B.2: Fraction of resolved turbulent kinetic energy for location 409. Panel (a) is the simulation with wave effects and panel (b) is the case without wave effects.